EXPERIMENTAL INVESTIGATION INTO THE ONSET OF STALL FLUTTER ON TILTROTOR BLADES

A.D. Croke*, D. Zagaglia, M.A. Woodgate, R.B Green, G.N. Barakos
James Watt School of Engineering, University of Glasgow
University Avenue, Glasgow, G12 8QQ, Scotland, UK
* Corresponding Author, e–mail: a.croke.1@research.gla.ac.uk

Abstract

A wind tunnel investigation into the stall of tiltrotor blades in propeller mode was undertaken. A custom blade set was instrumented with fully bridged axial strain gauges to monitor the flap bending strain at two radial locations. Propeller torque data was also analysed. The propeller was tested at varying blade pitch angles, advance ratios and rotational frequencies to clearly identify the blade stall boundary. Stall onset manifested in the strain results as a departure from linear behaviour of the bending strain versus pitch angle curves, an increase in the standard deviation of the strain gauge measurements, the presence of non-harmonic content in the strain spectra and a non consistent oscillation amplitude in the strain time history. For an increasing blade pitch angle, a sudden development of stall was found with variation in RPM as opposed to a more gradual onset as the advance ratio was increased.

Keywords: Propellers, Aerodynamics, Flow Separation, Stall Flutter, Wind Tunnel.

NOMENCLATURE

Acrynoms

AoA	Angle of Attack
CFD	Computational Fluid Dynamics
CSD	Computational Structural Dynamics
eVTOL	Electric Vertical Take-off and Landing
HMB3	Helicopter Multi-Block Code
MENtOR	Methods and Experiments for NOvel Rotorcraft
RPM	Revolutions Per Minute
UofG	University of Glasgow
UoM	University of Manchester
UKNRR	United Kingdom National Rotor Rig
UKVLN	United Kingdom Vertical Lift Network

Symbols

c_{tip}	Chord at blade tip, (m)
C_Q	Torque coefficient, $Q/\left(\rho n^2 D^5\right)$, $(-)$
D	Propeller diameter, (m)
f	Frequency, (Hz)
$\mathcal{F}(\cdot)$	Fourier transform of function $\cdot$
J	Advance ratio, $U_\infty/(nD)$, $(-)$
M_{tip}	Mach number at blade tip, $(-)$
n	Propeller rotational frequency, (Hz)
N_{rev}	Number of revolutions, $(-)$
R	Propeller radius, (m)
Re_{tip}	Reynolds number at blade tip, $2\pi n R c_{tip}/\nu$, $(-)$
U_∞	Freestream velocity, (m/s)
x	Blade radial coordinate, (m)
$\beta_{0.75R}$	Blade pitch angle at 75% radius, $(^\circ)$
$\overline{\epsilon_B}$	Bridge compensated strain, $(-)$
ϵ_B	Bridge uncompensated strain, $(-)$
ν	Kinematic viscosity, (m^2/s)
ρ	Air density, (kg/m^3)
Ω	Propeller rotational frequency, (RPM)

1. INTRODUCTION

The recent selection of the Bell V-280 tiltrotor aircraft by the United States Army as the replacement for the Sikorsky UH-60 Black Hawk and sudden growth in the development of electric Vertical Take-off and Landing (eVTOL) tiltrotor vehicles has lead to a significant research interest within the aerospace engineering community to qualify the operating envelope of tiltrotor blades[1]. Many of the proposed eVTOL configurations intend to operate as tiltrotor vehicles, therefore imposing the requirement of operating in both vertical and forward flight regimes. As a result, typical blades will be required to operate in unexplored regions of the flight envelope, potentially leading to the probing of aerodynamic and aeroelastic boundaries[2]. In addition, electric RPM regulated motors and modern composite blade designs which incorporate highly twisted and swept blade shapes are likely to alter the stall flutter boundary, thus increasing the likelihood of the phenomenon occurring.

Typically stall flutter manifests itself in rotating aerofoils such as propeller blades[3], helicopter rotors[4] and turbomachinery[5]. As defined by Dowell[6], stall flutter is recognised as partial or complete flow separation around the propeller blade which results in a periodic oscillation. In contrast to classical flutter, where the flow remains attached, stall flutter exhibits non-linear aerodynamic behaviour subsequently leading to an excitation of the propeller structure, consequently leading to a significant reduction of the flutter boundary.

Recent numerical works by Higgins et al.[7,8] has rejuvenated propeller stall flutter research. Using the high-fidelity Helicopter Multi-Block Code (HMB3) solver, Computational Fluid Dynamics (CFD) and Computational Structural Dynamics (CSD) tool packages have been coupled to investigate the aeroelastic response of a propeller both at attached and separated flow conditions[9,10,11]. The collection of works by Higgins et al. highlight that propeller stall flutter exhibits very strong three-dimensional aerodynamic effects and negative aerodynamic damping[12]. At conditions were detached flow was present, displays of pressure fluctuations occur, enhancing aeroelastic deformation of the propeller blade.

In contrast, a low-order model developed by Delamore-Sutcliffe et al.[13] is based upon an eigenvalue solution that assesses blade stability. A semi-empirical high-angle of attack unsteady aerodynamic model was coupled with a structural model to predict the stall flutter boundary. The method is demonstrated to successfully predict the stall flutter boundary and is validated using the experimental data of Baker[14].

Experimental efforts to adequately capture propeller stall flutter are extremely limited. The majority of investigations were undertaken prior to 1960, making use of blade sets with undefined structural and/or geometric properties. Immediately post the first world war, the growth in the manufacture of propeller aircraft was significant, also leading to a sizeable increase in propeller research. However, due to a large number of unexplained propeller blade failures[15], multiple experimental investigations into the bending and torsional deflections at large angles of attack were undertaken using novel optical techniques[16,17]. Hartman and Biermann[18] further investigated torsional and bending deflections using full-scale propellers at both static and low forward advancing conditions, typical of a propeller at the take-off or low speed phase of flight where blade stall and flutter will occur. Testing found the magnitude of torsional deflections at x/R = 0.7 to reduce with an increasing advance ratio. Explained by the larger relative velocity resulting in a reduced local Angle of Attack (AoA) for an equivalent lift. During flutter, load measurements became unsteady and there was a noticeable unfavourable shift in propeller coefficients of thrust and torque. A large audible sound was emitted during flutter, confirming an earlier prediction made by Stowell[19].

Further tests by Hartman and Biermann[20] demonstrated violent flutter at low advance resulting in a reduction of propulsive efficiency of up to 18%. Previous findings of Borck[21] nearly two decades earlier also support the explanation that flutter of propeller blades could potentially lead to the blade oscillating in and out of stall, as the local AoA varies as a function of time, resulting in a reduced propulsive efficiency. During the early 1940's investigations were undertaken both in the United Kingdom and United States to investigate propeller flutter of both attached and stalled flows. British testing[22,23,24,25] comprised of static and low advance inflow, fixed and variable pitch settings, and variable rotational speeds. The most commonly used technique to measure blade deformation was the placement of both axial and torsional strain gauges at various locations along the blade span and chord. Without the advantages of modern computing capabilities, strain gauge locations were determined using analytical methods such as the Rayleigh-Ritz method or cantilever beam theory.

Moreover, an array of additional experimental methods were also implemented such as stroboscopic imaging, acoustic arrays and the light-beam method, where a laser is reflected off of a mirror placed on the blade surface back towards photosensitive paper from which flutter amplitudes and frequencies could be extracted.

Despite a significant previous interest into propeller stall flutter, there is a clear lack of experimental data of sufficient resolution in the public domain that can be used to to validate newly developed high-fidelity methods whilst also providing further insight into the development of blade stall and stall flutter.

Prior campaigns are severely limited, with most experimental campaigns conducted prior to 1960, utilising novel (at the time) optical methods or instrumented blades with strain gauges where time histories were not adequately captured. Few attempts were made to capture load data and/or investigate the surrounding flow field. Despite significant amounts of experimental data collected, all of the propeller blades tested were wooden or metal-alloy models, with undefined structural and/or geometric properties, thus rendering the data collected as not suitable for validation of newly developed numerical models.

The purpose of this paper is to present strain gauge and torque data displaying the structural behaviour of a set of tiltrotor blades that is being characterised at the University of Glasgow. This will form part of a modern aeroelastic database that will be made available to validate numerical models but also provide an insight to blade stall development using state-of-the-art experimental apparatus.

Figure 1: The UKNRR installed in the DeHavilland tunnel.

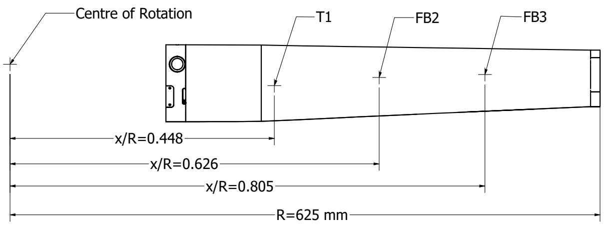

Figure 2: Location of flap bending (FB2, FB3) and torsional (T1) strain gauge bridges on the instrumented blade.

2. EXPERIMENTAL SETUP

2.1. United Kingdom National Rotor Rig

This investigation made use of the UK National Rotor Rig (UKNRR). As part of the EPSRC MENtOR project, undertaken within the UK Vertical Lift Network (UKVLN), the UKNRR was reconfigured from a fully articulated tiltrotor design to a conventional fixed-pitch propeller configuration. Reconfiguration took place at the University of Glasgow, to ensure the safe operation of a 1.25 m diameter Mach-scaled ($M_{tip} \approx 0.6$) propeller. The UKNRR allows for maximum permissible testing conditions of 3000 RPM, 3.4 kN of thrust and 350 Nm of torque. The motor that drives the propeller has a maximum available power of 125 kW. In order to test in propeller mode, the flap hinge, lead-lag hinge and the swashplate cyclic actuation were fixed by means of mechanical stops. Different blade pitch angles could be tested by adjusting the swashplate position along the shaft. A picture of the UKNRR in propeller mode inside the test section of the DeHavilland wind tunnel is shown in Figure 1. For further information about the rig, please refer to Zagaglia et al.[26].

2.2. DeHavilland Wind Tunnel

The experimental investigation was undertaken in the DeHavilland low-speed wind tunnel at The University of Glasgow (UofG). The DeHavilland wind tunnel is a low-speed closed return wind tunnel, with a 2.74m x 2.1m x 5m (Width x Height x Length) test section. The tunnel has a contraction ratio from the settling chamber to test section of 5:1. The tunnel can operate at a maximum freestream velocity (U_∞) of 70 m/s with an empty test section, and provides a uniform flow with a turbulence intensity of $<$ 0.2%. Due to the proximity of the propeller plane to the Pitot-Static probe that is usually used to set the wind tunnel speed, the pressure difference across the contraction section, once calibrated, was used as reference dynamic pressure. For further information about the wind tunnel calibration, please refer to Zagaglia et al.[26].

2.3. Instrumented Blades

Four composite tilt-rotor blades were custom designed at UofG[27] in the framework of the MENtOR project. The blade design has been adapted from an earlier blade set developed by The University of Manchester (UoM) to satisfy the new rig limitations as a result of modification to propeller mode. The blades incorporate the following blade sections: NACA 64_128 at the root ($x/R = 0.26$), Vertol V43015_2.48 ($x/R = 0.6$) and Vertol V23010_1.58 at the tip ($x/R = 1$). The blades have an overall, non linear twist of 19.3° and a root chord of 84.2 mm which is maintained constant up to $x/R = 0.43$ and then tapers to 60 mm at the tip.

Each blade is instrumented with fully bridged shear and axial strain gauges, totalling seven bridges per blade. Strain gauges were installed on the internal surface of the blade skin to allow for review of bridge time histories and spectral content of the blade structural response at various test points within the test matrix, and to provide an affirmation of stalled flow conditions within the test matrix.

Strain gauge bridges have been placed at various locations along the spanwise and chordwise directions, shown on Figure 2, to measure flap bending (FB), lead-lag bending (LB) and torsional twist (T). Bridge locations were determined during the design of the blade which made use of coupled CFD and CSD simulations[27].

Due to a large amount of collected data, this paper will focus on the two flap bending bridges, FB2 and FB3, which are located 390 mm (0.624R) and 503 mm (0.8R) from the propeller centre respectively. These bridges are composed of four axial strain gauges oriented in the spanwise direction, of which two gauges are co-located on the upper blade surface and two on the lower, at the same spanwise location. This full-bridge arrangement compensates for centrifugal loading and thermal deformation, so that the bridge reading ϵ_B is representative of the difference in flap bending strain between the upper and lower surface of the blade, $\epsilon_B = \epsilon_{LOW} - \epsilon_{UP}$.

Positive values of ϵ_B are to be expected when the blade is normally loaded (i.e. with moderately positive blade pitch angles) since ϵ_{UP} is negative (e.g. the upper fibres are compressed) and ϵ_{LOW} is positive (e.g. the bottom fibres are under tension).

Measurements of local bending and torsion are transmitted from the rotating frame of the rig to the stationary frame via a Datatel telemetry system. The strain time histories were sampled for a total of 19.5 s at a frequency of 6.7 kHz, allowing a frequency resolution for the spectra of approximately 0.05 Hz.

In order to correctly compare strains obtained at different flow densities and rotational speeds, a compensated strain measurement $\overline{\epsilon_B}$ will be used throughout this paper, defined as:

$$(1) \quad \overline{\epsilon_B} = \epsilon_B \frac{\overline{\rho}}{\rho} \left(\frac{\overline{\Omega}}{\Omega} \right)^2$$

where $\overline{\rho}$ is the reference density (i.e. 1.225 kg/m^3), $\overline{\Omega}$ is the reference rotational speed, i.e. 1800 RPM and ϵ_B is the non compensated bridge reading.

2.4. Torque Measurements

The propeller rig is endowed with a rotational shaft balance which at the time of testing was not yet fully commissioned. To estimate the blade torque, the feedback torque from the motor controller was used. This included other sources of torque other than the blade aerodynamic torque, such as internal frictions and the torque arising from the hub and spinner. To compensate for this, blade-off measurements at several rotational speed and advance ratios were acquired and subtracted to the corresponding blade-on measurements. Torque coefficients were computed using the standard definition for propellers:

$$(2) \quad C_Q = \frac{Q}{\rho n^2 D^5}$$

3. TEST MATRIX

The test matrix used to determine the stall boundary of this blade set was varied using three parameters: propeller rotational frequency Ω, advance ratio $J = U_\infty/(nD)$ and blade pitch $\beta_{0.75R}$ measured at 75% of the propeller radius. As the rotor has been configured to operate as a fixed pitch propeller, the pitch angle was fixed during each test with only rotational frequency and advance velocity varying.

Testing was performed at a range of blade pitch angles between $\beta_{0.75R} = 15.9^o$ to 35.6^o. All tests were performed for a range of rotational speeds between 1080 RPM and 1800 RPM in increments of 120 RPM. This corresponded to a maximum tip Mach number of $M_{tip} = 0.35$ and a maximum tip chord based Reynolds number of $Re_{tip} \approx 0.47$ million.

Due to the nature of the closed loop wind tunnel, in cases when the tunnel was not turned on (“No WT”), the propeller would still induce a recirculating flow around the tunnel loop that acted as a *de facto* advance velocity.

The magnitude of the recirculation is dependant on $\beta_{0.75R}$, as for attached cases an increasing blade pitch will result in a larger induced flow and therefore an increased advance ratio. "No WT" tests, when the wind tunnel fan was not turned on, were performed for every pitch angle to assess the minimum advance ratio at which the propeller could be tested. At "wind on" conditions the wind tunnel was turned on to introduce an oncoming wind to the propeller. Each test was run at constant advance ratio and pitch angle, requiring the magnitude of the wind tunnel speed to be adjusted as the propeller rotational speed was varied.

Moreover, for each blade pitch angle, the maximum advance ratio values that could be tested increased with blade pitch, as a higher $\beta_{0.75R}$ would allow for a larger reduction in the angle of attack caused by the advance speed before having negative thrust. The most outboard bending strain gauge, FB3, and the motor torque were monitored

Table 1: Test matrix as a function of blade pitch $\beta_{0.75R}$ and advance ratio J. Each test was performed at RPM varying from 1080 RPM to 1800 RPM in 120 RPM increments. X = Point tested, Blank = Point not tested.

$\beta_{0.75R}$	No WT	J=0.3	J=0.4	J=0.5	J=0.6	J=0.7	J=0.8	J=0.9	J=1.0	J=1.1	J=1.2	J=1.3	J=1.4
15.9°	X	X	X	X									
17.4°	X	X	X	X	X								
19.2°	X	X	X	X	X	X							
20.9°	X	X	X	X	X	X	X						
22.5°	X		X	X	X	X	X	X					
24.2°	X		X	X	X	X	X	X	X				
25.8°	X		X	X	X	X	X	X	X	X			
27.3°	X		X	X	X	X	X	X	X	X	X		
28.9°	X			X	X	X	X	X	X	X	X	X	
30.5°	X			X	X	X	X	X	X	X	X	X	X
32.2°	X			X	X	X	X	X	X	X	X	X	X
33.9°	X			X	X	X	X	X	X	X	X	X	X
35.6°	X			X	X	X	X	X	X	X	X	X	X

throughout testing to determine at what advance ratio the outboard section of the blade entered negative loading.The advance ratio was limited to 1.4 for the large pitch angle tests due to the maximum achievable wind tunnel speed. A visual representation of the test matrix is shown in Table 1.

4. RESULTS AND DISCUSSION

4.1. Identification of Stall Onset

As previously stated in section 3, the minimum speed at which the wind tunnel could be set was dependent on the magnitude of the recirculation around the tunnel loop caused by the propeller. Figure 3 shows the advance ratio induced by such recirculation when the tunnel was not turned on as a function of the propeller rotational frequency, for a series of blade pitch angles. At low $\beta_{0.75R}$, the induced advance ratio is constant with respect to Ω, implying that the propeller works at constant thrust coefficient throughout the range of RPM investigated. As the blade pitch is increased, the J curves move upwards as the thrust grows. They also start to bend down in the low RPM range, until they collapse on one another, e.g in the range 22.5° $\leq \beta_{0.75R} \leq$ 30.5° at 1080 RPM. This is evidence that the thrust generated by the propeller stops to grow, suggesting the onset of stall; it is expected for stall to affect low RPM cases first as the lower blade Reynolds number promotes flow separation at lower AoAs. As the pitch angle is further increased, the collapse point moves to higher RPMs, suggesting that stall starts to affect cases with higher blade Reynolds numbers also.

Stall onset can also be appreciated by looking at the strain measurements. Figure 4(a) shows the compensated strain for bridges FB2 and FB3 at 1080 RPM in the "No WT" case, as a function of the blade pitch angle. FB2 and FB3 are flap bending bridges

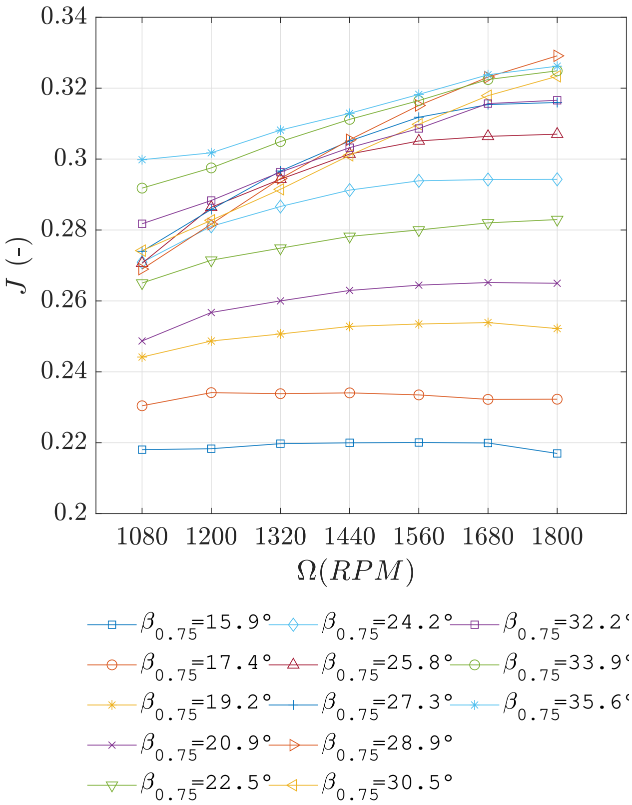

Figure 3: Propeller induced J vs RPM at "No WT" condition, for various pitch settings.

positioned at $x/R = 0.62$ and $x/R = 0.8$ respectively. Since the flapping motion of the blade was constrained by flap stops, the blade acted as a cantilever beam, hence readings for FB2 which is closer to the root, were generally higher than those for FB3. A departure from linear behaviour can be appreciated for both bridges starting at $\beta_{0.75R} = 22.5°$, marking the stall onset at this rotational speed, as already appreciated when looking at the advance ratio curves of Fig. 3 collapsing on one another. This is further confirmed by looking at the standard deviation of the bridge measurements (represented as an error bar in Figure 4(a)), that sees a sharp increase in magnitude for $\beta_{0.75R} \geq 22.5°$, owing to the much more unsteady aerodynamics of the stalled blades. Considering that the bending bridges measure the strain caused by the overall load acting from their position until the end of the blade (i.e. $0.8 \leq x/R \leq 1$ for FB3 and $0.62 \leq x/R \leq 1$ for FB2), and after the stall onset both FB2 and FB3 readings drop by roughly the same amount, this suggests that most of the stall develops towards the blade tip.

The effect of varying the advance speed on the FB2 reading is shown in Figure 5(a) at 1080 RPM and Figure 5(b) at 1800 RPM. It should be reminded that the ”No WT” curve, differently from the other ones, was not obtained at constant advance ratio, as this would depend on the specific pitch setting ($0.22 \leq J \leq 0.3$ for 1080 RPM and $0.22 \leq J \leq 0.33$ for 1800). For both rotational frequencies, before stall, an increase in forward speed causes a decrease in the bending reading, as the effective AoA the blade is subjected to decreases. This also causes the stall angle to increase for larger advance speeds, as the peak of the strain curve moves to larger $\beta_{0.75R}$. At an equal advance ratio, the stall angle is always smaller in the 1080 RPM case (Figure 5(a)) with respect to the 1800 RPM case (Figure 5(b)), reinforcing again the idea that low RPM propellers tend to stall sooner, even at larger advance ratios.

This can also be appreciated from Figure 6(b), where the compensated FB2 readings are plotted against the pitch angle for several RPM settings at J=0.5, showing the stall angle moving to higher values as the RPM is increased. It should be noted that if the strain data were not compensated, the curves for different Ω would be on completely different scales due to the change in the dynamic pressure seen by the blade, hence different loading. By applying the compensation, we are effectively comparing the results as if the same dynamic pressure were present on the blades. In the not stalled region this allows us to appreciate the centrifugal stiffening of the blades, that causes smaller compensated deformations for larger rotational speeds.

To further indicate the presence of stall, analysis of the strain spectral content and its time history was undertaken and presented in Figure 7 for $\beta_{0.75R} = 30.5^o$. Figure 7(a) clearly displays a large non-harmonic content across a broadband of frequencies for both 1080 and 1800 RPM, superimposed to the underlying propeller harmonics at multiple integers of its rotational frequency. Alternatively, Figure 7(b) presents the same rotational frequencies and blade pitch, however for an increased advance ratio of 0.5. Upon inspection, it is clear that the 1080 RPM case exhibits a similar behaviour to that of the corresponding "No WT" case (Figure 7(a)), whereas the 1800 RPM does not appear to show a large broadband content and is represented by the propeller harmonics only. This can be explained by the propeller not being stalled for the 1800 RPM case. It is expected that the spectral content of a propeller blade operating at a stalled condition will exhibit a significant non-harmonic content, where the signal energy is distributed amongst a large range of frequencies. This behaviour is driven by stall cells being shed in the wake at frequencies that are not necessarily synchronised with the propeller harmonics. Opposingly, a propeller rotating in a non-stalled condition should mainly display a content that is comprised of the fundamental frequency and its harmonics.

To corroborate this observation, the time histories of the strain signals over 20 revolutions are shown in Figures 7(c) and 7(d). It is clear that whenever the blade is stalled, no repeatable pattern and consistency in the amplitude of the oscillation can be found in the time histories, with aperiodic bursts. Conversely, upon inspection of the 1800 RPM case at J = 0.5, Figure 7(d), the signal clearly shows a repetitive pattern of consistent amplitude, as the 1/rev signal is apparent as a prominent downwards spike at equally spaced time intervals. These observation on the time histories and spectra of stalled and not stalled cases ware found to be valid also for all the other cases not directly presented here, hence giving a reliable criterion to identify the presence of stall.

Further insight on the stall development can be achieved though analysis of the torque. Figure 8 presents the torque coefficient as a function of the advance ratio for several blade pitch angles, at two different rotational frequencies. Until stall, all curves behave as expected, with a gradual reduction in propeller torque for an increasing advance ratio as the effective AoA of the blade is decreased, resulting in a reduced thrust and therefore a reduced induced power. Moreover, an increase in the blade pitch angle promotes a consistent shift to larger torque values, with the curves almost evenly spaced. In the

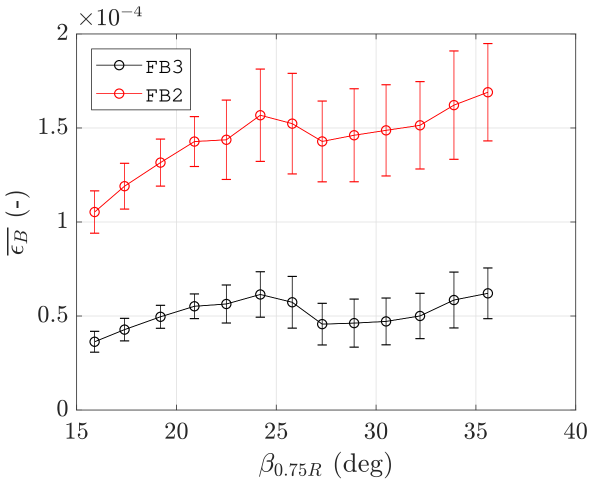

(a) No WT

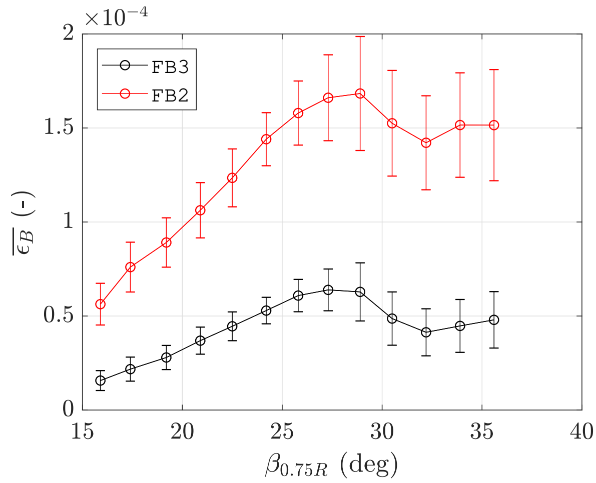

(b) J=0.5

Figure 4: Compensated strain for bridges FB2 and FB3 at 1080 RPM as a function of the blade pitch angle. Standard deviation of the measurements has been added as error bar.

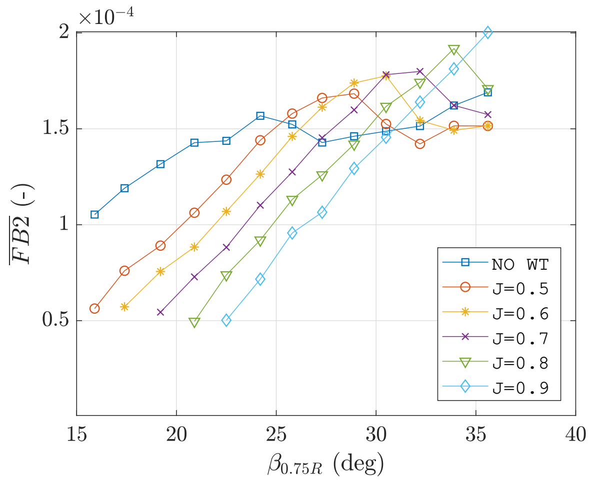

(a) Ω = 1080 RPM

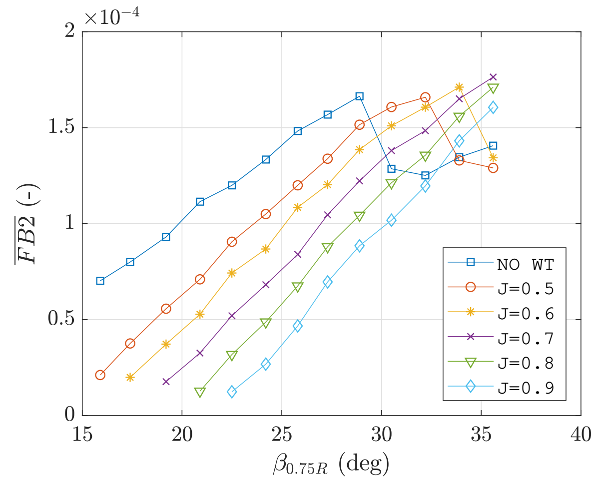

(b) Ω= 1800 RPM

Figure 5: Compensated strain for bridge FB2 as a function of the blade pitch angle for various J.

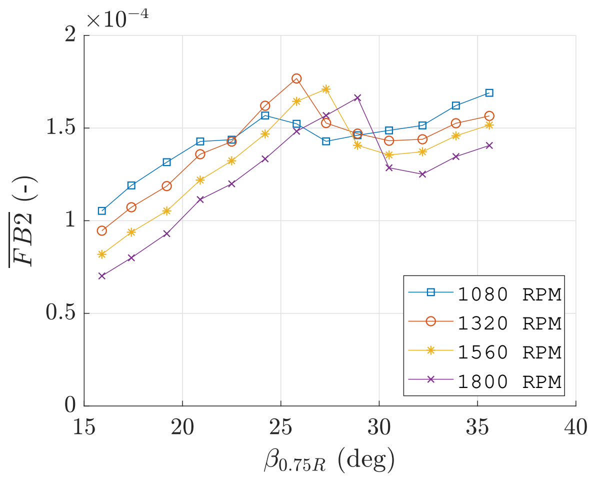

(a) No WT

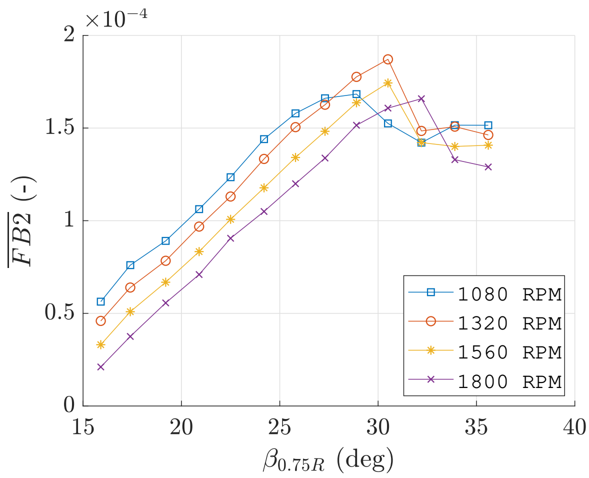

(b) J=0.5

Figure 6: Compensated strain for bridge FB2 as a function of the blade pitch angle for various RPM.

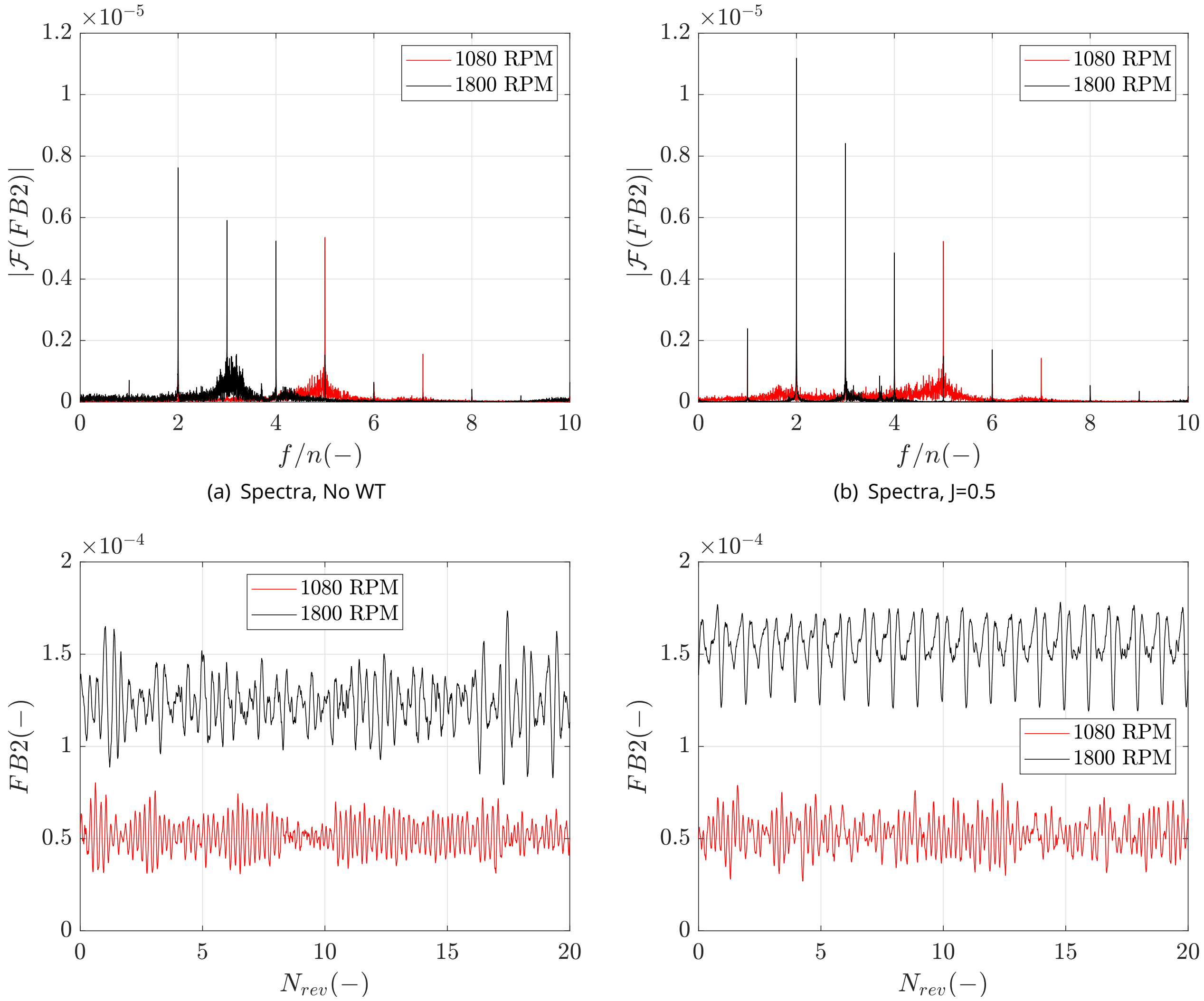

(a) Spectra, No WT

(b) Spectra, J=0.5

(c) Time history, No WT

(d) Time history, J=0.5

Figure 7: Amplitude of the Fourier transform (as a function of the non dimensional frequency f/n) and time histories (as a function of the number of revolutions) of the uncompensated strain measurements for FB2 at $\beta_{0.75R} = 30.5°$.

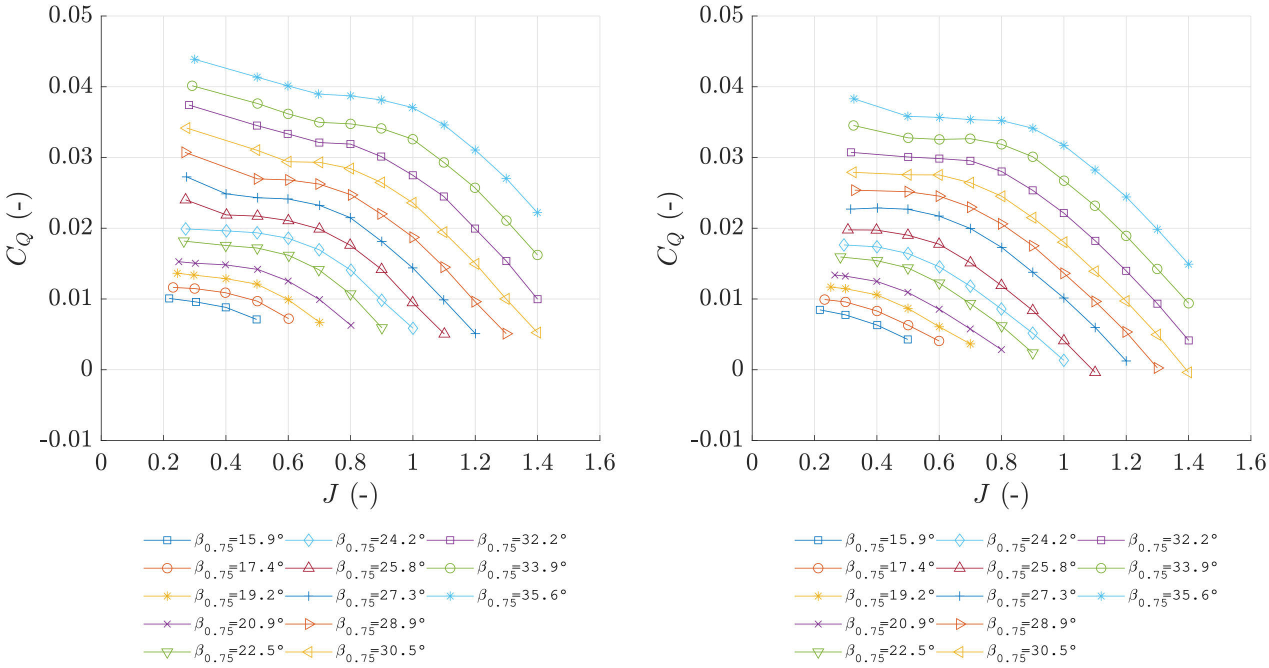

(a) Ω = 1080 RPM (b) Ω= 1800 RPM

Figure 8: Torque coefficient C_Q as a function of the advance ratio J, various pitch settings.

top-left corner of both plots, where the stalled cases are present, a large change in the slope of the $C_Q - J$ curves can be observed as opposed to the flat behaviour of the curves for the non-stalled cases. This can be explained by the large increase in passive drag arising from the stalled regions. However, not all the stalled cases show a noticeable variation in slope in that region. For example, at 1080 RPM, all cases with $\beta_{0.75R} \geq 22.5°$ at sufficiently low J have been identified as stalled cases using the other criteria adopted up to this point. However, the curves for $\beta_{0.75R} = 22.5°$ and 24.2° in Figure 8(a) do not show a remarkable change in gradient. This is believed to be caused by the increase in passive power being partially compensated for by a decrease in the induced power due to a reduction in thrust at stall onset. Hence while a strong change in the slope can be effectively be used to assess the presence of fully developed stall in a particular test point, early-stage stall might still be present in cases that show no such behaviour.

4.2. Stall Boundaries

As detailed in section 4.1, stall has been identified at a variety of test points within the test matrix, using the following criteria:

- Collapse of the induced velocity when increasing the pitch angle.
- Departure from linear behaviour of the bending strain vs blade pitch curves.
- Increase in the standard deviation of the strain gauge measurements.
- Presence of non-harmonic content in the strain spectra.
- Non consistent oscillation amplitude in the strain time history.
- Sudden increase in torque for fully developed stall (even if not so evident at stall onset).

Testing was performed at varying rotational frequencies Ω, advance ratios J and blade pitch angles $\beta_{0.75R}$ as described in section 3 to characterise the stall envelope of the tiltrotor blade set. The overall test points and the subset of cases where stall was identified using the criteria above are presented in Figure 9. Although not the focus of this paper, it should be noted that cases at high advance ratio were also investigated to qualify the opposite end of the propeller operational envelope, where the negative angle of attack induced by the advance speed creates negative thrust towards the blade tip. The maximum advance ratio that could be tested increased with the blade pitch angle. Therefore, $\beta_{0.75R} = 15.9^o$ could be tested up to and including J = 0.5, while $\beta_{0.75R} \geq 30.5^o$ could be tested up to and including J = 1.4.

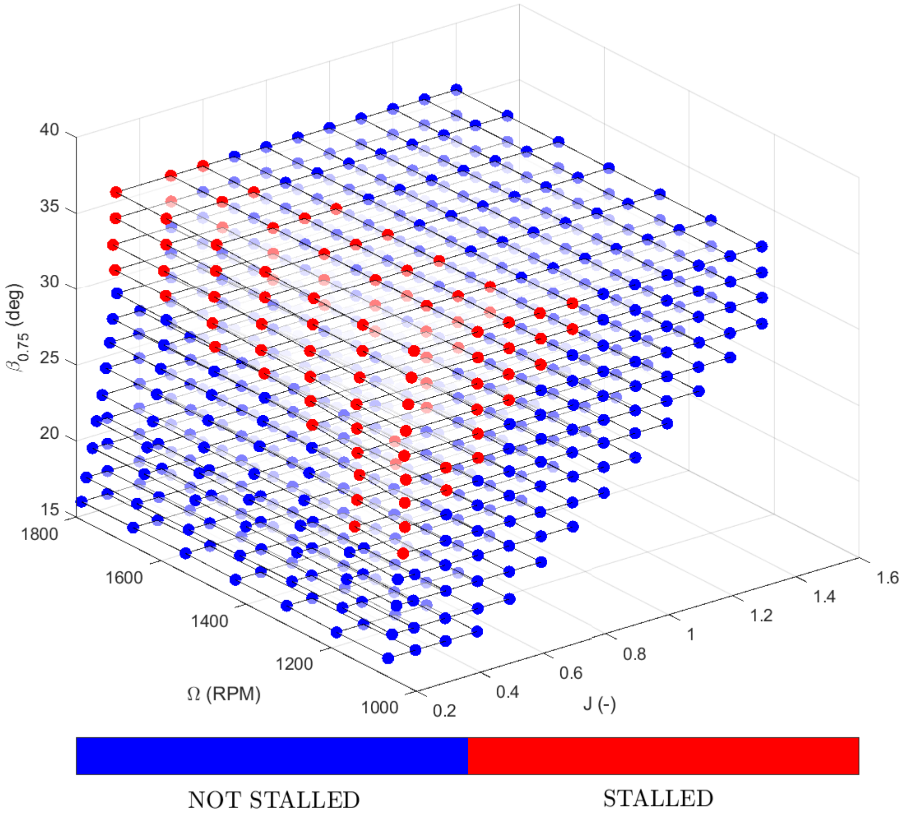

Figure 9: Stall boundary, as a function of rotational speed, advance ratio and blade pitch angle. Each dot correspond to a test point: red indicates evidence of stall, blue otherwise.

By looking at Figure 9, stall was primarily observed at a lower advance ratio, lower rotational frequencies and large blade pitch angles, as expected.

The smallest pitch angle at which stall was identified was $\beta_{0.75R} = 22.5^o$ during a "No WT" test performed at a corresponding J = 0.265 at and 1080 RPM, with all cases prior to this showing no evidence of stalled flow. However, it is clear that looking at $\beta_{0.75R} = 22.5^o$ and 24.2^o at 1080 RPM and 1200 RPM, both indicate presence of early onset of stall as even a small increase in advance ratio to J = 0.4 results in the re-attachment of the flow.

As $\beta_{0.75R}$ was increased, the number of rotational frequencies at which stall was present for low advance ratios grew in a discontinuous manner. For the "No WT" cases between 22.5° $\leq \beta_{0.75R} \leq$ 27.3°, stall was only present at $\Omega \leq$ 1200 RPM. At $\beta_{0.75R} =$ 28.9°, there was a sudden growth in rotational frequencies at which stall was present up to 1560 RPM. Eventually, for $\beta_{0.75R} \geq$ 28.5°, stall was present at all Ω tested, up to and including 1800 RPM. This sudden growth in the range of RPMs at which stall is present is a direct consequence of the effect of the Reynolds number on stall development: for how large the Reynolds number can be, there will be always a point when the AoA will be excessive and stall will develop.

This behaviour was observed for both the "No WT" case, where a small variation in J was present by varying the RPM, and for J=0.4 and J=0.5, where J was kept constant across the RPM range.

On the contrary, the influence of J on the presence of stall was observed to be more gradual and approximately linear. At 1080 RPM, the minimum J at which stall was observed varied from 0.25 at $\beta_{0.75R} =$ 22.5° to 0.8 at $\beta_{0.75R} =$ 35.6°. Similar gradual behaviour was observed at higher RPM values, even if for a smaller range of J and pitch angles, as the volume of stalled points reduces in size.

5. CONCLUSIONS

A wind tunnel investigation into tiltrotor blade stall was presented. A custom blade set was instrumented with fully bridged axial strain gauges to monitor the flap bending strain at two radial location. Propeller torque data was also analysed. The propeller was tested at varying blade pitch angles, advance ratios and rotational frequencies to clearly identify the blade stall boundary.

1. Stall onset was identified using the following criteria: collapse of the induced velocity when increasing the pitch angle, departure from linear behaviour of the bending strain vs blade pitch curves, increase in the standard deviation of the strain gauge measurements, presence of non-harmonic content in the strain spectra and non consistent oscillation amplitude in the strain time history.

2. A sudden increase in torque was clear for fully developed stall. However, this was not overly apparent at stall onset, meaning that torque information alone could not solely be used to identify the presence of stall in its early stages.

3. As the blade pitch angle was increased, development of stall was observed to be more sudden in nature when varying the RPM (and therefore the blade critical Reynolds number) as opposed to a more gradual onset when the advance ratio was increased.

This investigation serves as a baseline for future experimental testing to further understand the aerodynamics of stalled propellers and identify stall flutter boundaries.

ACKNOWLEDGMENTS

The authors would like to acknowledge the technical assistance provided by Dr David J. Pickles.

This research is part-funded by the U.K. Research Council (EPSRC) Methods and Experiments for Rotorcraft (MENtOR), Grant EP/S013814/1, and part-funded by Dowty Propellers project in conjunction with the University of Glasgow, Numerical and Experimental Study of Propeller Aeroelasticity (NESPA).

REFERENCES

[1] Filippone, A. and Barakos, G. N., “Rotorcraft systems for urban air mobility: A reality check,” *The Aeronautical journal*, Vol. 125, (1283), 2021, pp. 3–21.

[2] Appleton, W., Filippone, A., and Bojdo, N., “Interaction effects on the conversion corridor of tiltrotor aircraft,” *The Aeronautical Journal*, Vol. 125, (1294), 2021, pp. 2065–2086.

[3] Higgins, R., Barakos, G., and Filippone, A., “A review of propeller stall flutter,” *The Aeronautical Journal*, Vol. 126, (1304), 2022, pp. 1678–1717.

[4] Leishman, G. J., *Principles of Helicopter Aerodynamics*, Cambridge University Press, 2006.

[5] Rowe, J. and Mendelson, A., “Experimental Investigation of Blade Flutter in an Annular Cascade,” Techincal Note 3581, National Advisory Committee for Aeronautics, Washington, D.C, USA, 1955.

[6] Dowell, E. H., Curtiss, H. C., Scanlan, R. H., and Sisto, F., *A Modern Course in Aeroelasticity*, Springer, 1995.

[7] Higgins, R. J., *Investigation of Propeller Stall Flutter*, Ph.D. thesis, University of Glasgow, Glasgow, Scotland, Apr 2021.

[8] Higgins, R. J. and Barakos, G. N., “Whirl and Stall Flutter Simulation Using CFD,” 43rd European Rotorcraft Forum, Milan, Italy, 12-15 Sep 2017.

[9] Higgins, R., Jimenez-Garcia, A., Barakos, G. N., and Bown, N., “A Time-Marching Aeroelastic Method Applied to Propeller Flutter,” AIAA Scitech 2019 Forum, San Diego, CA, USA, 7-11 Jan 2019.

[10] Higgins, R. J., Jimenez-Garcia, A., Barakos, G. N., and Bown, N., “High-Fidelity Computational Fluid Dynamics Methods for the Simulation of Propeller Stall Flutter,” *AIAA Journal*, Vol. 57, (12), 2019, pp. 5281–5292.

[11] Higgins, R. J., Barakos, G. N., Jinks, E., and Bown, N., “A Propeller Blade Design for Experimental Stall Flutter Investigations,” 47th European Rotorcraft Forum, Virtual Meeting, 6-9 Sep 2021.

[12] Higgins, R. J., Barakos, G. N., and Jinks, E., “Estimation of three-dimensional aerodynamic damping using CFD,” *Aeronautical journal*, Vol. 124, (1271), 2020, pp. 24–43.

[13] Delamore-Sutcliffe, D. and Greenwell, D., “A Model for the Fast Prediction of Propeller Stall Flutter,” 24th AIAA Applied Aerodynamics Conference, San Francisco, CA, USA, 5-8 Jun 2006.

[14] Baker, J. E., “The effects of various parameters, including mach number, on propeller-blade flutter with emphasis on stall flutter,” Techincal Note 3357, National Advisory Committee for Aeronautics, Langley Air Force Base, VA, USA, 1955.

[15] Seewald, F., “Flutter in propeller blades,” Techincal Memorandum 642, National Advisory Committee for Aeronautics, Washington, D.C, USA, 1931.

[16] Liebers, F., “Resonance vibrations of aircraft propellers,” Techincal Memorandum 657, National Advisory Committee for Aeronautics, Washington, D.C, USA, 1932.

[17] Theodorsen, T., “Propeller vibrations and the effect of the centrifugal force,” Techincal Note 516, National Advisory Committee for Aeronautics, Langley Field, VA, USA, 1935.

[18] Hartman, E. P. and Biermann, D., “The torsional and bending deflection of full-scale

aluminium-alloy propeller blades under normal operating conditions," Report 644, National Advisory Committee for Aeronautics, Langley Field, VA, USA, 1938.

[19] Stowell, E. Z. and Deming, A. F., "Noise from two-blade propellers," Report 526, National Advisory Committee for Aeronautics, Langley Field, VA, USA, 1936.

[20] Hartman, E. P. and Biermann, D., "The effect of compressibility on eight full-scale propellers operating in the take-off and climbing range," Report 639, National Advisory Committee for Aeronautics, Langley Field, VA, USA, 1938.

[21] Borck, H., "Dependence of propeller efficiency on angle of attack of a propeller blade," Technical Memorandum 54, National Advisory Committee for Aeronautics, Langley Field, VA, USA, 1921.

[22] Shannon, J. and J.R.Forshaw, "Propeller blade vibration: Nature and severity of vibration at edgewise resonance as influenced by coupling effects due to blade twist," Reports & Memoranda 2561, Aeronautical Research Council, London, England, UK, 1941.

[23] Clifton, F. and Sterne, L., "Strain Gauge Test of a Fluttering Propeller in a Wind Tunnel," Reports & Memoranda 2072, Aeronautical Research Council, London, England, UK, 1943.

[24] Sterne, L. and Brown, R., "The Elimination of Flutter from a Propeller," Reports & Memoranda 2047, Aeronautical Research Council, London, England, UK, 1943.

[25] Sterne, L., "Spinning tests on fluttering propellers," Reports & Memoranda 2022, Aeronautical Research Council, London, England, UK, 1945.

[26] Zagaglia, D., Croke, A. D., Green, R. B., and Barakos, G. N., "Development of the UK National Rotor Rig for aeroelastic testing of rotary wings," 49th European Rotorcraft Forum, Bückeburg, Germany, 05-07 Sep 2023.

[27] Woodgate, M. A., Fitzgibbon, T. A., and Barakos, G., "The Use of Computational Fluid Dynamics in the Investigation of Stall Onset on Tilt-Rotor Blades," 47th European Rotorcraft Forum, Virtual Meeting, 6-9 Sep 2021.